Capacitance Computation of Elliptic Microstrip Disks in Biaxial Anisotropic Multilayered Substrates

RAFAEL R. BOIX AND MANUEL HORNO, MEMBER, IEEE

Abstract—**Variational technique in the spectral domain are used to develop an algorithm which calculates a lower bound of the capacitance of a conductor elliptic disk embedded in a lossless multilayered substrate with arbitrary dielectric anisotropy. This algorithm is intended to be a useful tool for lumped element design in MMIC applications. The calculation method is shown to be general, quick, and accurate when implemented in a computer program. Numerical results are given to demonstrate the efficiency of the algorithm.**

I. INTRODUCTION

LUMPED ELEMENT circuits offer an attractive alternative to distributed circuits in MMIC's. Lumped elements are of relatively small size and thanks to this, they make it possible to reduce the semiconductor area wasted in passive circuits. For design purposes, it is necessary to develop computer programs to characterize such type of elements [1].

Microstrip patches with an arbitrary shape are commonly used as lumped elements. Many papers have been published dealing with the calculation of the capacitance of such patches. Special attention has been paid to the analysis of the circular patch. A complete bibliographical report on the calculation of the capacitance of a circular conductor plate in homogeneous and inhomogeneous media can be found in [2]. A modified version of the circular patch is the elliptic patch. It appears that very little work has been done on the determination of the capacitance of elliptic microstrip patches including fringing field effects. Besides, the only capacitance data for elliptic patches we have been able to find are not very reliable [3]. This will be proved in this paper.

The capacitance values of elliptic microstrip patches can be used in the analysis of elliptic microstrip resonators to account for fringe effects. By means of these capacitance values, it is possible to derive effective dimensions and effective permittivities, which can be included in a modified cavity model to obtain the resonance frequencies [3], [4]. This model is much less time-consuming in a computer than a full-wave analysis [5]. The elliptic resonator presents some advantages over the simpler circular resonator. For instance, it can be used in the design of parametric amplifiers and harmonic multipliers by varying the eccentricity as a degree of freedom [6]. Also, no mode splitting due to slight deformations occurs in the elliptic resonator and the field configuration is fixed with respect to the axes [3].

The modified cavity model can also be used to analyze elliptical microstrip antennas. Circular and rectangular microstrip antennas can be adapted to provide circular polarization, but multiple feeds are needed. However, by using a slightly elliptical radiator, it is possible to obtain circular polarization while retaining a simple feed. This fact has been proved by means of analytical work [7] and experimental measurements [8].

All the results reported on the calculation of the capacitance of circular and elliptic microstrip disks deal with the conventional microstrip configuration in which the conductor plate is printed on a single isotropic dielectric [2], [3]. In this paper, we provide an algorithm to determine the capacitance of an elliptic conductor plate embedded in a multilayered anisotropic substrate. Multilayered analysis allows the study of configurations in which several dielectric layers are involved (e.g., suspended, inverted, and sandwiched configurations) and it also allows the simulation of dielectrics with a continuous permittivity variation in one direction. The effect of anisotropy is also taken into account because a variety of practical substrates are anisotropic and serious errors may be incurred when anisotropy is neglected [9]. Variational techniques in the spectral domain are employed in an adequate way to compute the value of the capacitance of the elliptic plate. Once implemented in a computer program, the algorithm developed turns out to be general, accurate, and quick.

II. VARIATIONAL FORMULATION FOR THE CAPACITANCE OF THE ELLIPTIC DISK

In Fig. 1(a), we have drawn the cross section of a stratified medium composed of N layers of lossless anisotropic dielectric materials. An infinitely thin and lossless elliptic conductor plate lies between the Mth and $(M+1)$th dielectric layers. The dimensions of the ellipse and its orientation referred to the coordinate system cho-

Manuscript received March 15, 1989; revised August 11, 1989. This work was supported by the DGICYT under Project PB87-0798-C03-01

The authors are with the Departamento de Electronica y Electromagnetismo, Facultad de Fisica, Universidad de Sevilla, Av. Reina Mercedes s/n., 41012-Sevilla, Spain.

IEEE Log Number 8931555.

0018-9480/90/0100-0030$01.00 ©1990 IEEE

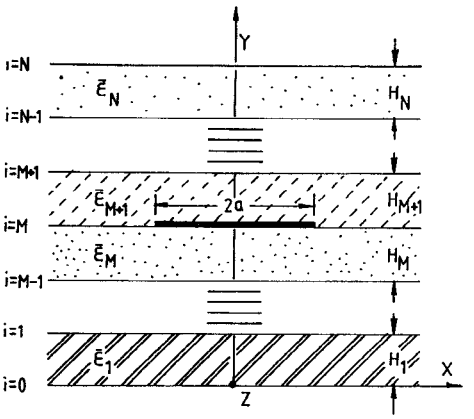

(a)

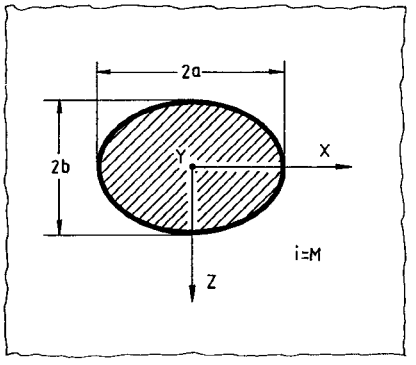

(b)

Fig. 1. (a) Multilayered substrate with biaxial dielectric anisotropy. (b) Elliptic conductor patch placed at the Mth interface of the multilayered substrate shown in (a).

sen are given in Fig. 1(b). The eccentricity of the ellipse is given by

$$e = \left(1-(b/a)^2\right)^{1/2}. \tag{1}$$

Dielectric materials in the multilayered configuration are allowed to present biaxial anisotropy, and their permittivity tensors can be expressed as

$$\bar{\epsilon}_i = \epsilon_0 \begin{bmatrix} \epsilon^*_{11,i} & \epsilon^*_{12,i} & \epsilon^*_{13,i} \\ \epsilon^*_{12,i} & \epsilon^*_{22,i} & \epsilon^*_{23,i} \\ \epsilon^*_{13,i} & \epsilon^*_{23,i} & \epsilon^*_{33,i} \end{bmatrix} \qquad (i=1,\cdots,N). \tag{2}$$

The six independent parameters of the permittivity tensor can be expressed in terms of its eigenvalues $\epsilon^*_{x,i}$, $\epsilon^*_{y,i}$, and $\epsilon^*_{z,i}$ and the Euler angles ϕ_i, θ_i, and ψ_i, which describe the position of the tensor principal axes referred to the Cartesian coordinate axes shown in Fig. 1(a) and (b) [10]. Boundary interfaces $i=0$ and $i=N$ are independently allowed to be any one of three different possibilities: electric walls, magnetic walls, or open boundaries extending to infinity.

When a two-dimensional Fourier transform is carried out from the spatial variables $X-Z$ to the spectral variables $\alpha-\beta$, the electric energy associated with the structure shown in Fig. 1(a) can be expressed as [10]

$$U = \frac{1}{8\pi^2}\int_{-\infty}^{+\infty}\int_{-\infty}^{+\infty} G(\alpha,\beta)\left|\tilde{\rho}(\alpha,\beta)\right|^2 d\alpha\, d\beta. \tag{3}$$

In the above expression, $\tilde{\rho}(\alpha,\beta)$ stands for the two-dimensional Fourier transform of the charge density on the elliptic conductor plate and $G(\alpha,\beta)$ is the spectral Green's function. For a multilayered dielectric substrate with biaxial anisotropy, the value of $G(\alpha,\beta)$ is obtained by means of a recurrent algorithm proposed in [10]. The spectral Green's function dependence on the Fourier variables α and β is expressed in terms of hyperbolic functions as is written below:

$$G(\alpha,\beta) = G\left(F_i(\alpha,\beta)\coth\left(H_iF_i(\alpha,\beta)\right), F_i(\alpha,\beta)\right.$$
$$\left.\cdot\operatorname{cosech}\left(H_iF_i(\alpha,\beta)\right)\right) \qquad \text{(in general, } i=0,\cdots,N+1\text{)} \tag{4a}$$

where

$$F_i(\alpha,\beta) = (1/\epsilon^*_{22,i})\Big[\left(\epsilon^*_{22,i}\epsilon^*_{11,i}-(\epsilon_{12,i})^2\right)\alpha^2 + \left(\epsilon^*_{22,i}\epsilon^*_{33,i}-(\epsilon^*_{23,i})^2\right)\beta^2 + 2\left(\epsilon^*_{13,i}\epsilon^*_{22,i}-\epsilon^*_{12,i}\epsilon^*_{23,i}\right)\alpha\beta\Big]^{1/2}. \tag{4b}$$

Owing to Thomson's theorem, the right-hand side of (3) provides an upper bound for the electric energy if an approximated expression is used for the transformed charge density $\tilde{\rho}(\alpha,\beta)$ on the elliptic plate. This means that the charge density needs to be previously estimated in the spatial domain to obtain a stationary value of U.

At this point, it is necessary to choose an adequate coordinate system to express the charge density on the plate. Considering the geometry of the problem, the natural coordinates to be used are the orthogonal elliptic coordinates (ξ,η,y) defined in [11]. In general, for an elliptic plate embedded in an arbitrary multilayered anisotropic substrate, the charge density depends on both variables ξ and η. When the dielectrics present uniaxial anisotropy and their optical axis are aligned with the Y axis defined in Fig. 1(a) (i.e., $\epsilon^*_{11,i}=\epsilon^*_{33,i}$ and $\epsilon^*_{12,i}=\epsilon^*_{13,i}=\epsilon^*_{23,i}=0$), the electrostatic potential for the problem and the charge density on the plate no longer depend on the η variable. Nevertheless, the use of the variables ξ and η to approximate the charge density is unsuitable when a transformation to the two-dimensional Fourier space is attempted to obtain $\tilde{\rho}(\alpha,\beta)$. To avoid this, adifferent choice for the coordinate system has been made. The coordinates employed are related to the natural coordinates used in the problem of the circular plate (limiting case of an elliptic plate with vanishing eccentricity), which are cylindrical coordinates (r,ϕ,y) [12]. By analogy with cylindrical coordinates (r,ϕ,y), we define the coordinate system (r',ϕ',y) for the more general problem of the elliptic plate with nonvanishing eccentricity as

$$x = r'\cos\phi'$$
$$z = (b/a)r'\sin\phi'. \tag{5}$$

The points on the elliptic plate are obtained by varying the coordinates defined in (5) through the range $0<r'<a$,

$0 < \phi' < 2\pi$, $y = \sum_{i=1}^{M} H_i$. This coordinate system is not orthogonal unless $b = a$, and in this latter case, it represents the cylindrical coordinate system. In our analysis, we use the coordinates defined in (5) and we assume that the charge density on the elliptic plate depends only on r'. As will be seen below, this choice makes it possible to obtain the two-dimensional Fourier transform of the charge density in a way which is suitable for calculating the electric energy via expression (3). The assumption $\rho = \rho(r')$ is only true for the case of a circular plate embedded in a multilayered anisotropic substrate with circular symmetry;i.e., dielectrics must have uniaxial anisotropy and the optical axes must be aligned and perpendicular to the interfaces. For the more general case of an elliptic plate embedded in an arbitrary anisotropic substrate, the assumption is not valid since the charge density on the plate also depends on the ϕ' coordinate. However, the effects of complex anisotropy and nonvanishing eccentricity can be regarded as perturbations of the simple case of a circular plate on an aligned uniaxial substrate. Considering this, the mentioned assumption can be interpreted as a first-order approximation for the real charge density. The smaller the eccentricity and the weaker the anisotropy, the better the approximation will be. Also, it should be taken into account that if some error is made in the approximation of the charge density, this error is reduced when the electric energy of the structure is calculated, owing to the variational features of expression (3).

Besides the spatial coordinate transformation proposed in (5), we also substitute the variables α and β in the two-dimensional transformed space by a pair of new variables, γ and Ω, given by

$$\alpha = \gamma \cos \Omega$$
$$\beta = (a/b)\gamma \sin \Omega. \tag{6}$$

When the variable transformations shown in (5) and (6) are introduced in the definition of the two-dimensional Fourier transform of the charge density on the elliptic plate, this can be written as

$$\tilde{\rho}(\gamma) = \frac{2\pi b}{a} \int_0^a J_0(\gamma r') \rho(r') r' dr'. \tag{7}$$

As a result of the assumption $\rho = \rho(r')$, the charge density transform depends only on the γ variable in the transformed space. It can be noticed that the integral appearing in (7) stands for the zeroth-order Hankel transform of the function $\rho(r')$ [12]. When the new variables defined in (6) are introduced in (3), the electric energy can be rewritten as

$$U = \frac{a}{8\pi^2 b} \int_0^{2\pi} \int_0^{\infty} G(\gamma, \Omega) [\tilde{\rho}(\gamma)]^2 \gamma d\gamma d\Omega. \tag{8}$$

In this expression $\tilde{\rho}(\gamma)$ is a real quantity owing to the definition given in (7). The spectral Green's function generally depends on the variables γ and Ω, as can be derived when (6) is introduced in (4b). When the problem to be solved presents circular symmetry, the spectral Green's function no longer depends on Ω and only a single integral has to be carried out in (8).

The charge density approximation on the plate is optimized by using trial function expansions. Therefore, the charge density can be written as

$$\rho(r') = \sum_{i=0}^{p} a_i \rho_i(r'). \tag{9}$$

When (9) is introduced in (7) and the result is substituted in (8), the energy turns out to be a function of the unknown coefficients a_i. These coefficients are obtained by minimizing the electric energy, being the total charge conditioned to be a constant on the plate. This constant is chosen to be equal to 1 without loss of generality. To solve the isoperimetric problem that arises, Lagrange's multipliers method is applied. As a result of these calculations, a set of linear equations is obtained:

$$\left.\begin{aligned} \sum_{i=0}^{p} a\Gamma_{ij} + \lambda Q_j &= 0 \\ \sum_{i=0}^{p} a_i Q_i &= 1 \end{aligned}\right\} \quad (j = 0, \cdots, p) \tag{10}$$

in which the coefficients Γ_{ij} are given by

$$\Gamma_{ij} = \frac{a}{8\pi^2 b} \int_0^{2\pi} \int_0^{\infty} G(\gamma, \Omega) \tilde{\rho}_i(\gamma) \tilde{\rho}_j(\gamma) \gamma d\gamma d\Omega \quad (i, j = 0, \cdots, p). \tag{11}$$

The coefficients $Q_i = \tilde{\rho}_i(\gamma = 0)$ stand for the contribution of each trial function to the total charge on the plate and the unknown "λ" is the Lagrange's multiplier. By using the system of equations (10), the electric energy can be rewritten in a very simple way, namely,

$$U = \sum_{i=0}^{p} \sum_{j=0}^{p} a_i a_j \Gamma_{ij} = -\lambda. \tag{12}$$

Since the total charge on the plate is taken to be equal to 1, the capacitance will be given by $C = 1/2U$. Therefore, the charge density approximation on the plate provides an upper bound for the exact value of the electric energy, and it also provides a lower bound for the exact value of the capacitance. The use of Lagrange's multipliers method ensures the calculation of a lower bound for the capacitance. This point is not considered by Leong *et al.* in their analysis [13], and although the method employed by them is variational, no lower bound for the capacitance is obtained (see Maxwell's distribution results in [13, table 1].

III. Trial Functions for the Charge Density

Option 1

As a first approximation, a uniform charge distribution is assumed on the elliptic plate, namely

$$\rho(r') = \begin{cases} 1, & r' \leqslant a \\ 0, & r' > a. \end{cases} \tag{13}$$

This approximation was the one employed by Sharma *et al.* in [3]. In fact, when the charge distribution shown in (13) is introduced in our formulation, the capacitance

TABLE I
NORMALIZED CAPACITANCE $CH/\pi\epsilon_0\epsilon_r a^2$ OF MICROSTRIP CIRCULAR DISK AS A FUNCTION OF THE RATIO DISK RADIUS/SUBSTRATE THICKNESS (a/H) FOR $\epsilon_r = 1$ AND $\epsilon_r = 2.65$

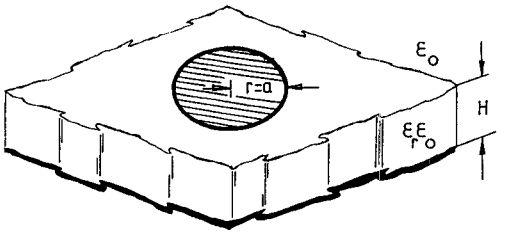

Normalized capacitance $CH/(\pi\epsilon\epsilon_r a^2)$

a/H	Ref. [16]	Variational Ref. [13]	Variational This method	Ref. [16]	Variational Ref. [13]	Variational This method	Number of Trial Functions
		$\epsilon_r = 1$			$\epsilon_r = 2.65$		
0.1	----	26.3006	26.3006	----	18.2310	18.2310	2
0.2	----	13.5920	13.5920	----	9.4866	9.4866	2
1.0	3.5346	3.5345	3.5346	2.6122	2.6121	2.6122	3
2.0	2.3183	2.3179	2.3183	1.8100	1.8094	1.8100	3
10.0	1.3180	1.3159	1.3180	1.1809	1.1780	1.1809	4
20.0	1.1756	----	1.1756	1.0969	----	1.0969	4
100.0	1.0421	----	1.0440	1.0210	----	1.0228	6

The results are compared with those provided in [13] and [16]. Option 2 is used for the calculation of the capacitance. The number of trial functions used to ensure convergence in each case is given.

expression obtained for an elliptic patch on a single isotropic substrate is mathematically equivalent to that reported in [3]; therefore, it should yield the same results. For the case of the circular microstrip patch, it has been reported that the constant charge density approximation provides reliable results only for high values of the ratio disk radius/substrate thickness [13], [14]. For practical values of this ratio, the range of error produced by this approximation varies between 4 and 8 percent [13]. By analogy, the range of error arising in the case of an elliptic patch must be similar. This will be ascertained in the results section. When (7) is applied, the transform of the function appearing in (13) turns out to be

$$\tilde{\rho}(\gamma) = 2\pi b \frac{J_1(\gamma a)}{\gamma}. \tag{14}$$

This result allows us to recognize the infinite series appearing in [3, eq. (13)] and evaluate those series by using the simple numerical expressions given in [15] for Bessel functions.

Option 2

In this case, we employ an expansion of the form

$$\rho(r') = \sum_{i=0}^{p} a_i \frac{T_{2i}(r'/a)}{\left(1-(r'/a)^2\right)^{1/2}} \tag{15}$$

where $T_{2i}(x)$ are Chebyshev polynomials of the first kind.

As can be seen, each term in the expansion accounts for the charge density singularity at the edge. This sort of trial functions has been successfully employed in the analysis of microstrip rectangular patches [10]. The first term in the expansion represents Maxwell's charge distribution, which has also been used in the calculation of the capacitance of a circular microstrip plate [12]–[14]. In that case, Maxwell's distribution is reported to provide accurate results for small values of the disk radius/substrate thickness ratio. It will be seen below that for larger values of this ratio, higher order terms in the expansion given in (15) make it possible to spread the validity range of the one term approximation. In fact, a small number of trial functions in (15) yield accurate results for our purposes in the range of practical dimensions for both circular and elliptic patches. The transform of the functions appearing in (15) is given by

$$\tilde{\rho}_i(\gamma) = \frac{\pi^2 ba}{2}\left[J_{(i-1/2)}\left(\frac{\gamma a}{2}\right)J_{-(i-1/2)}\left(\frac{\gamma a}{2}\right) + J_{(i+1/2)}\left(\frac{\gamma a}{2}\right)J_{-(i+1/2)}\left(\frac{\gamma a}{2}\right)\right] \qquad (i=0,\cdots,p). \tag{16}$$

Bessel functions of integer order plus one half appear in (16). Functions of this type are expressed in terms of simple trigonometric functions that are quickly computed. The numerical evaluation of the integrals appearing in (11) for the trial functions chosen in options 1 and 2 has been accelerated by means of an analytical treatment. This is explained in detail in the Appendix.

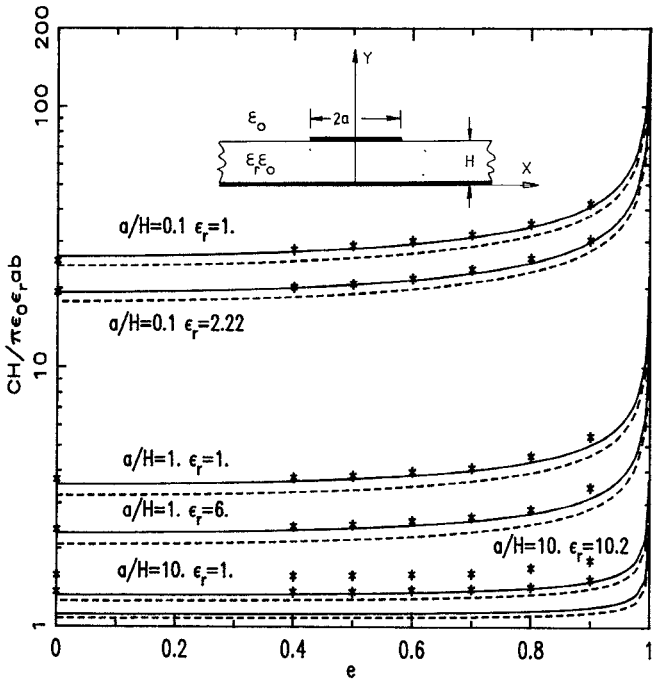

Fig. 2. Normalized capacitance of a microstrip elliptic disk as a function of eccentricity for different values of the major axis/substrate thickness (a/H) ratio and for different permittivities. Solid lines are used for option 2 results and dashed lines are used for option 1. The asterisks correspond to the results given in [3, fig. 8].

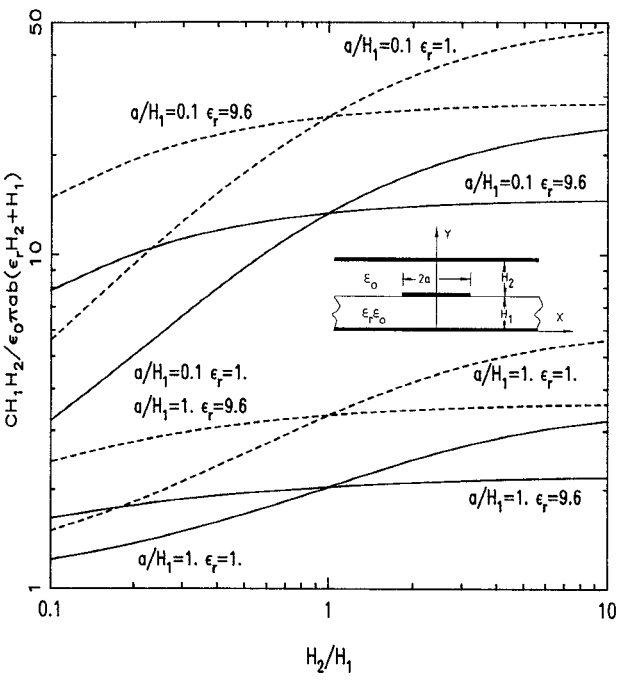

Fig. 3. Capacitance of an elliptic microstrip disk with shielding upper ground plane (normalized to the capacitance obtained by ignoring the fringing fields) as a function of the relative position of the plane. Solid lines stand for zero eccentricity and dashed lines stand for nonzero eccentricity ($b/a = 0.3$).

IV. Results

Two programs were implemented for the calculation of the capacitance of circular and elliptic plates in multilayered and anisotropic substrates. One of them works on structures showing circular symmetry, in which numerical integrals with respect to the Ω variable in (11) do not have to be performed. The other program can treat nonsymmetrical structures involving elliptic plates on arbitrary anisotropic substrates.

The accuracy of the algorithm was first checked by comparing our results with very exact existing data for the capacitance of circular microstrip disks in vacuum and circular disks printed on a single dielectric slab [13], [16]. Values are presented in Table I for a wide range of variation of the disk radius/substrate thickness ratio. It can be seen that as this ratio increases, the number of trial functions required in option 2 to obtain a precise result also increases. For large values of the ratio mentioned, the variational algorithm presented in [13] does not seem to be as accurate as the one presented here.

In Fig. 2, the normalized capacitance of an elliptic microstrip disk is plotted versus eccentricity. The results obtained with the two options given in Section III for the charge density approximation are shown. It is clear from the figure that the capacitance values calculated with option 2 enhance considerably those obtained with option 1. The difference between the data corresponding to each option varies between 4 and 9 percent. This difference becomes higher as both the plate surface/substrate thickness ratio and the substrate permittivity decrease. The asterisks in Fig. 2 stand for the results obtained in [3, Fig. 8] by Sharma *et al.* As was stated in Section III, these authors employ a uniform charge density distribution function on the elliptic plate in their formulation; therefore, their results should coincide with those presented here for option 1. However, serious discrepancies are noticed. To check the validity of both groups of results, a comparison was made with the results reported in [12] and [13] in the limit of vanishing eccentricity, keeping the assumption of constant charge distribution on the plates. We found that our results agree closely with the mentioned data, whereas Sharma's results provide errors ranging from 5 to 25 percent, which increase as the major axis/substrate thickness ratio increases. Looking at Fig. 2, these error percentages seem to remain for nonvanishing eccentricities. The formulation presented in [3] is similar to that presented here for option 1, but the numerical treatment is much more cumbersome, since it requires carrying out two iterated integrals over an infinite interval, and the function to be integrated is calculated by evaluating a slowly convergent series. Owing to this, we think that serious numerical errors were made to generate the results given in [3], and these results should not be considered to be reliable.

In Fig. 3, the effect of the shielding upper ground plane on the capacitance of microstrip circular and elliptic disks is analyzed. As can be seen, this effect is stronger as the ratio plate surface/substrate thickness decreases and as the substrate permittivity decreases.

In Fig. 4, even- and odd-mode capacitances of broadside coupled microstrip circular and elliptic disks on anisotropic substrates are plotted as a function of the distance between the conductor plates. From the figure, it can be derived

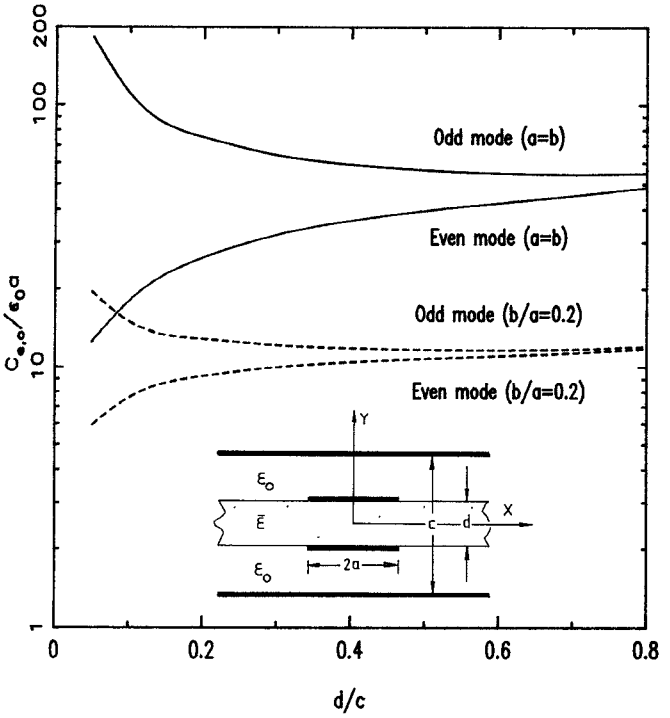

Fig. 4. Modal capacitances of broadside coupled elliptic and circular microstrip disks versus the relative thickness of the substrate ($a/c = 0.1$ is used in all the graphs). Solid lines stand for circular disks on sapphire substrate ($\epsilon_{11}^* = \epsilon_{33}^* = 9.4$; $\epsilon_{22}^* = 11.6$; $\epsilon_{12}^* = \epsilon_{13}^* = \epsilon_{23}^* = 0$). Dashed lines stand for elliptic disks on P.B.N. substrate ($\epsilon_{11}^* = \epsilon_{33}^* = 5.12$; $\epsilon_{22}^* = 3.4$; $\epsilon_{12}^* = \epsilon_{13}^* = \epsilon_{23}^* = 0$).

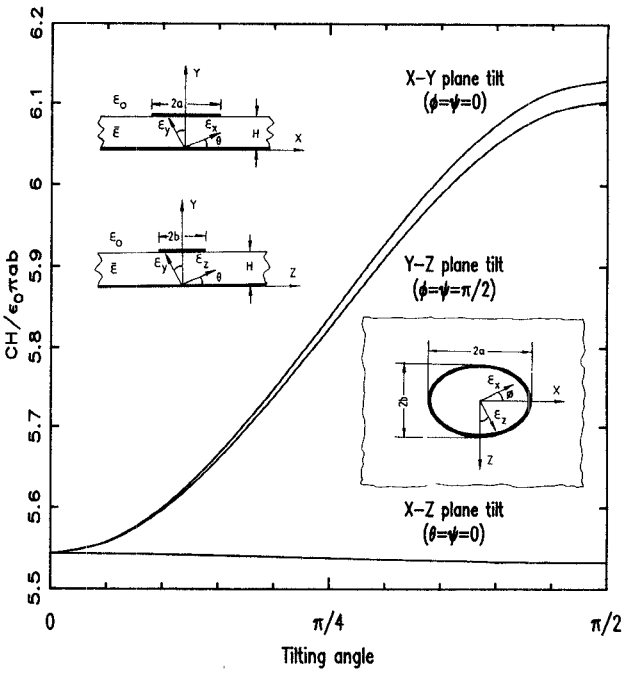

Fig. 5. Normalized capacitance of elliptic microstrip disk on anisotropic PTFE substrate ($a/H = 3$; $b/H = 0.9$; $\epsilon_x^* = 2.89$; $\epsilon_y^* = 2.45$; $\epsilon_z^* = 2.95$) as a function of the tilting angle between the principal axes of permittivity tensor and the coordinate axes defined in Fig. 1(a) and (b). Tilts in the three coordinate planes are studied.

that for a given distance between plates, the coupling is higher for a higher plate surface and for higher substrate permittivity.

In Fig. 5, the effect of biaxial anisotropy on the capacitance of an elliptic microstrip patch is studied. Normalized capacitance is plotted versus the angles between the principal axes of the permittivity tensor and the coordinate axes. The principal axes of the permittivity tensor are separately allowed to be tilted in the three coordinate plates, this tilt being expressed in terms of Euler's angles. The effect of tilting is very slight in the $X-Z$ plane since anisotropic PTFE presents little anisotropy in this plane. However, it is important in the $X-Y$ and $Y-Z$ planes, in which the normalized capacitance changes about 20 percent when the tilting angle varies from 0 to $\pi/2$.

In Fig. 6 is shown the normalized capacitance of an elliptic microstrip disk printed on an inhomogeneous dielectric with a varying permittivity in the Y direction as a function of the value of the permittivity at the ground plane. The permittivity is taken to be constant at the plane on which the conductor plate lies and it decays exponentially toward the ground plane. The variation is smaller as the permittivity at the ground plane increases. The continuously varying permittivity has been simulated by using N dielectric layers of equal thickness and constant permittivity. The value of the permittivity in each layer follows the exponential variation proposed ($N = 20$ was considered to be enough to obtain convergence in the capacitance value). According to the figure, the effect of inhomogeneity is

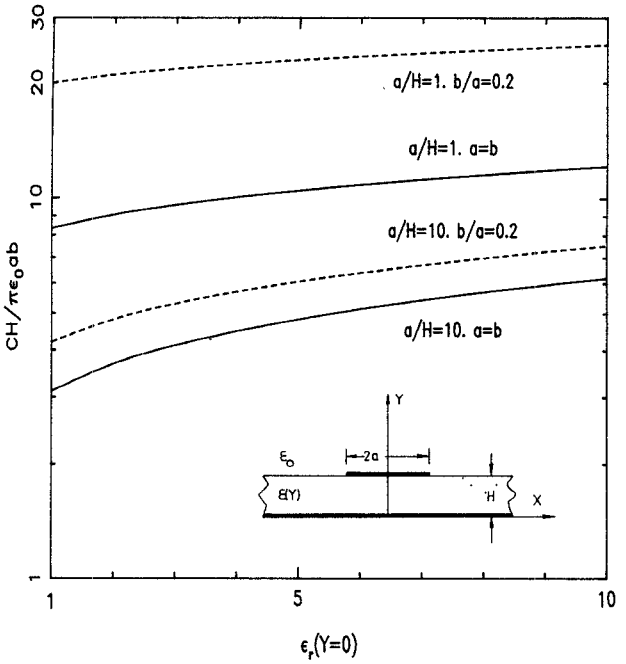

Fig. 6. Normalized capacitance of elliptic microstrip disk printed on a substrate with a variable permittivity in the Y direction. The capacitance is plotted versus the value of the permittivity at the ground plane $\epsilon(y = 0)$. The value of the permittivity is taken to be constant at the interface on which conductors lie $\epsilon(y = H) = 10$ and it decays exponentially toward the ground plane. Solid lines stand for zero eccentricity and dashed lines stand for nonzero eccentricity.

stronger for larger plates, in which the energy density is more confined in the region under the conductor plates.

V. Conclusions

An algorithm is developed for calculating the capacitance of an elliptic conductor patch embedded in a stratified substrate composed of lossless dielectric layers with arbitrary anisotropy. A variational expression in the spectral domain is used to compute a lower bound for the patch capacitance. Both the choice of an adequate spatial coordinate system and the use of a variable transformation in the two-dimensional Fourier space make it possible to account for the edge singularity in the approximation of the charge density on the elliptic plate. Because to this, the results obtained are quite accurate. A detailed analytical study of the integrals arising in the calculation of the capacitance makes it possible to increase the convergence speed of the algorithm when it is implemented in a computer program. Comparison with available data in the literature shows very good agreement in the limit of vanishing eccentricity. Original design graphs are presented with special emphasis on the use of inhomogeneous and anisotropic substrates.

Appendix

When the charge density transforms calculated in (14) and (16) are introduced in (11), the numerical evaluation of the infinite integrals with respect to the variable is slow since the integrands converge as $O(\gamma^{(-2)})$ for $\gamma \to \infty$. To accelerate convergence, we have made use of the asymptotic properties of the spectral Green's function $G(\gamma, \Omega)$. As was seen in (4a), $G(\gamma, \Omega)$ depends on the variable through hyperbolic functions. These functions exponentially reach their asymptotic limit for small values of their arguments. In fact, the asymptotic limit of $G(\gamma, \Omega)$ for the configuration shown in Fig. 1(a) is reached when $\min_{i=1,\cdots,N}(\gamma H_i) \approx 5$ and it turns out to be

$$\begin{aligned} G(\gamma,\Omega)|_{as} = \Big\{ & \epsilon_0 \gamma \Big[\left(\epsilon^*_{22,M}\epsilon^*_{11,M} - (\epsilon^*_{12,M})^2\right)\cos^2\Omega \\ & + \left(\epsilon^*_{22,M}\epsilon^*_{33,M} - (\epsilon^*_{23,M})^2\right)(a/b)^2 \sin^2\Omega \\ & + 2\left(\epsilon^*_{13,M}\epsilon^*_{22,M} - \epsilon^*_{12,M}\epsilon^*_{23,M}\right) \\ & \cdot (a/b)\sin\Omega\cos\Omega \Big]^{1/2} \\ & + \epsilon_0 \gamma \Big[\left(\epsilon^*_{22,M+1}\epsilon^*_{11,M+1} - (\epsilon^*_{12,M+1})^2\right)\cos^2\Omega \\ & + \left(\epsilon^*_{22,M+1}\epsilon^*_{33,M+1} - (\epsilon^*_{23,M+1})^2\right) \\ & \cdot (a/b)^2 \sin^2\Omega \\ & + 2\left(\epsilon^*_{13,M+1}\epsilon^*_{22,M+1} - \epsilon^*_{12,M+1}\epsilon^*_{23,M+1}\right) \\ & \cdot (a/b)\sin\Omega\cos\Omega \Big]^{1/2} \Big\}^{-1}. \end{aligned} \tag{A1}$$

This asymptotic expression provides the spectral Green's function for an elliptic plate placed between two semi-infinite media with permittivity tensors $\bar{\epsilon}_M$ and $\bar{\epsilon}_{(M+1)}$. Bearing in mind that $G(\gamma, \Omega)$ quickly reaches its asymptotic limit, we can rearrange the right-hand side of expression (11) in the following way:

$$\begin{aligned} \Gamma_{ij} = \frac{a}{8\pi^2 b} \Big\{ & \int_0^{2\pi}\int_0^{\infty} \left[\gamma G(\gamma,\Omega) \right. \\ & \left. - \gamma G(\gamma,\Omega)|_{as}\right] \tilde{\rho}_i(\gamma)\tilde{\rho}_j(\gamma)\, d\gamma\, d\Omega \\ & + A_{ij}\int_0^{2\pi} \gamma G(\gamma,\Omega)|_{as}\, d\Omega \Big\} \qquad (i,j=0,\cdots,p) \end{aligned} \tag{A2}$$

where

$$A_{ij} = \int_0^{\infty} \tilde{\rho}_i(\gamma)\tilde{\rho}_j(\gamma)\, d\gamma. \tag{A3}$$

The first infinite integral appearing in (A2) can be efficiently computed since the integrand decays exponentially. Concerning the second infinite integral, which is defined in (A3), we were able to obtain its value in closed form for the trial functions defined in Section III. So, for option 1,

$$A_{00} = \frac{16\pi ab^2}{3} \tag{A4}$$

and for option 2,

$$\begin{aligned} A_{ij} = \frac{\pi^4 b^2 a}{2}\left[I_{i-1,j-1} + I_{i-1,j} + I_{i,j-1} + I_{ij}\right] \\ (i,j=0,\cdots,p) \end{aligned} \tag{A5}$$

where

$$\begin{aligned} I_{nm} = \int_0^{\infty} & J_{(n+1/2)}(x) J_{-(n+1/2)}(x) J_{(m+1/2)}(x) \\ & \cdot J_{-(m+1/2)}(x)\, dx \qquad (n,m \geq -1). \end{aligned} \tag{A6}$$

For the case $n \geq m \geq 0$, we can write

$$I_{nm} = \frac{1}{\pi}\int_0^1 P_n(2t^2-1) P_m(2t^2-1)\, dt \tag{A7}$$

where Parseval's identity and [17, eq. (6.672.2)] have been applied. $P_n(x)$ are Legendre polynomials. By using the variable transformation $u = 1-2t^2$ and [17, eq. (7.232)], (A7) can be rewritten as

$$\begin{aligned} I_{nm} &= \frac{(-1)^{n+m}}{2\sqrt{2}\pi}\int_{-1}^{+1} \frac{P_n(u)P_m(u)}{(1-u)^{1/2}}\, du \\ &= \frac{(-1)^{n+m}}{(2n+1)\pi}\, {}_4F_3\left(-m, m+1, \frac{1}{2}, \frac{1}{2}; 1, n+\frac{3}{2}, \frac{1}{2}-n; 1\right) \\ &= \frac{2(-1)^{n+m}}{\pi} \\ &\quad \cdot \sum_{j=0}^{m} \frac{(m+j)!\left[(2j)\right]^2 (n+j+1)!\left[2(n-j)\right]!}{(m-j)!\left[(j)!\right]^4 (n-j)!\left[2(n+j+1)\right]!}. \end{aligned} \tag{A8}$$

For the rest of the values of n and m, the following relations have to be used:

$$I_{mn} = I_{nm} \tag{A9a}$$

$$I_{m,-1} = I_{mo} \qquad (m \geq -1). \tag{A9b}$$

As can be derived from (4b), the integrals with respect to the variable in (A2) have only to be performed between

0 and π, owing to the symmetrical dependence of the spectral Green's function on the α and β variables. When the condition $\epsilon_{13}^{*}\epsilon_{22}^{*} - \epsilon_{12}^{*}\epsilon_{23}^{*} = 0$ is fulfilled for each dielectric in the multilayered substrates, it is sufficient to integrate between 0 and $\pi/2$.

REFERENCES

[1] M. Caulton, B. Hershenov, S. P. Knight, and R. E. DeBrecht, "Status of lumped elements in microwave integrated circuits—present and future," *IEEE Trans. Microwave Theory Tech.*, vol. MTT-19, pp. 588–599, July 1971.

[2] E. F. Kuester, "Explicit approximations for the static capacitance of a microstrip patch of arbitrary shape," *J. Electromagnetic Waves Appl.*, vol. 2, no. 1, pp. 103–135, 1987.

[3] A. K. Sharma and B. Bhat, "Spectral Domain analysis of elliptic microstrip disk resonators," *IEEE Trans. Microwave Theory Tech.*, vol. MTT-28, pp. 573–576, June 1980.

[4] T. Itoh and R. Mittra, "Analysis of a microstrip disk resonator," *Arch. Elek. Übertragung.*, vol. 27, pp. 456–458, Nov. 1973.

[5] K. Araki and T. Itoh, "Hankel transform domain analysis of open circular microstrip radiating structures," *IEEE Trans. Antennas Propagat.* vol. AP-29, pp. 84–89, Jan. 1981.

[6] R. T. Irish, "Elliptic resonator and its use in microcircuit systems," *Electron. Lett.*, vol. 7, no. 7, pp. 149–150, Apr. 1971.

[7] L. C. Shen, "The elliptical microstrip antenna with circular polarization," *IEEE Trans. Antennas Propagat.*, vol. AP-29, pp. 90–94, 1981.

[8] S. A. Long, L. C. Shen, D. H. Schaubert, and F. G. Farrar, "An experimental study of the circular-polarized elliptical printed-circuit antenna," *IEEE Trans. Antennas Propagat.*, vol. AP-29, pp. 95–99, 1981.

[9] N. G. Alexópoulos, "Integrated circuit structures on anisotropic substrates," *IEEE Trans. Microwave Theory Tech.*, vol. MTT-33, pp. 847–881, Oct. 1985.

[10] R. R. Boix and M. Horno, "Lumped capacitance and open end effects of striplike structures in multilayered and anisotropic substrates," *IEEE Trans. Microwave Theory Tech.*, vol. 37, pp. 1523–1528, Oct. 1989.

[11] J. G. Kretzschmar, "Wave propagation in hollow conducting elliptical waveguides," *IEEE Trans. Microwave Theory Tech.*, vol. MTT-18, pp. 547–554, Sept. 1970.

[12] T. Itoh and R. Mittra, "A new method for calculating the capacitance of a circular disk for microwave integrated circuits," *IEEE Trans. Microwave Theory Tech.*, vol. MTT-21, pp. 431–432, June 1972.

[13] M. S. Leong, P. S. Kooi, and K. P. Heo, "Determination of circular microstrip disk by Noble's variational method," *Proc. Inst. Elec. Eng.*, pt. H, vol. 128, no. 3, pp. 306–310, Dec. 1981.

[14] S. Coen and Graham M. L. Gladwell, "A Legendre approximation method for the circular mistrostrip disk problem," *IEEE Trans. Microwave Theory Tech.*, vol. MTT-25, pp. 1–6, Jan. 1977.

[15] M. Abramowitz and J. A. Stegun, *Handbook of Mathematical Functions*. New York: Dover, 1964.

[16] K. Hongo and M. Takahashi, "Evaluation of integrals occurring in the study of circular microstrip disk," *IEEE Trans. Microwave Theory Tech.*, vol. MTT-30, pp. 1279–1282, Aug. 1982.

[17] I. S. Gradshteyn and I. M. Ryzhik, *Tables of Integrals, Series and Products*. New York: Academic Press, 1965.

✠

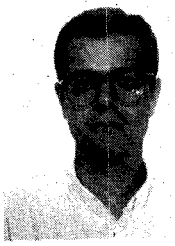

Rafael R. Boix was born in Melilla, Spain, on September 10, 1962. He received the B.Sc. and M.Sc. degrees in physics (Electronics Division) from Seville University in 1985 and 1986 respectively. Currently, he is working towards the Ph.D. degree at Seville University. His research interests include distributed and lumped microstrip circuit design and numerical methods in electromagnetism.

✠

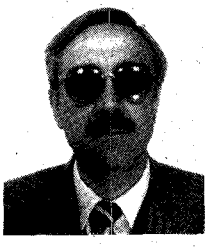

Manuel Horno (M'75) was born in Torre del Campo (Jaen), Spain. He received the M.Sc. degree in physics in June 1969, and the Ph.D. degree in physics in January 1972, both from Seville University, Seville, Spain.

Since October 1969 he has been with the Department of Electronics and Electromagnetism at Seville University, where he became an Assistant Professor in 1970, an Associate Professor in 1975, and Professor in 1986. His main fields of interest include boundary value problems in electromagnetic theory, wave propagation in anisotropic media, and microwave integrated circuits. He is presently engaged in the analysis of planar multiconductor transmission lines and lumped elements embedded in anisotropic substrate. He is also interested in the study of planar slow-wave structures with semiconductor and ferrimagnetic materials.